Coulombically Driven Rolling of Nanorods on Water

Lela Vuković and Petr Král*

Department of Chemistry, University of Illinois at Chicago, Chicago, Illinois 60607, USA

(Received 20 July 2009; published 10 December 2009)

We use molecular dynamics simulations to examine the possibility of rolling nanorods on the surfaces of polar liquids. Asymmetric charging of nanorod surfaces, generated by light excitation of its photoactive hydrophobic surfactants, can induce asymmetric Coulombic coupling to the polar liquid surfaces. We demonstrate that under this driving nanorods with diameters of 3–10 nm can roll on water with translational velocities of 1–5 nm/ns. The efficiency of this motion is controlled by the chemistry and dynamical phenomena at the nanorod-water interface.

DOI: 10.1103/PhysRevLett.103.246103 PACS numbers: 68.08.−p, 05.70.Np, 81.07.Nb, 83.50.Lh

Transport of nanoscale cargo at the cellular level is an essential part of everyday activity in all biosystems [1]. Motor proteins, such as kinesin [2], dynein [3], or myosin [4] can translate molecules and micelles along tubulous filaments in cells. Analogous manipulation of nanoscale objects in various media becomes necessary in modern technologies [5–7]. Although light tweezers [8] and other drag techniques [9] could be used to move and assemble nanoscale objects, future nanosystems might need to move autonomously and perform other activities. Locomotion of nanoscale objects in fluids might be stabilized by the medium. The power necessary for their motion can be delivered externally [10,11].

We examine the possibility of rolling nanorods [12] on the water surface. To this goal, (i) their rotation should be efficiently powered, (ii) they need to couple well to the water surface (not solvate) to become propelled with minimal slipping [13] (gravity is negligible), and (iii) their dynamics should be optimized and controlled, since their motility in fluids is limited by low Reynolds numbers; scallop theorem does not allow nanoscale propulsion to be realized by reversible mechanical means [14]. In principle, this rolling motion could be driven by synthetic molecular motors [15] and various ratchetlike mechanisms [16] with pulsating electrical or optical fields. In digital fluidics, polarizable water microdroplets are propelled on solid surfaces by electrostatic fields generated by buried electrodes [17]. Here, we propose to *invert* this approach and roll nanorods on the water surface, when their surface is asymmetrically polarized by light.

In Fig. 1, we show a model of such nanorod, briefly called a ''roller'', which is electrically driven to roll on the water surface. In reality, a metallic nanorod can be covered with triblock surfactants, bound to the metal core in the first (alkanethiol) block. The second block can be made of partially oriented and photoactive chromophores, which may extend into the third block, composed of alkane chains, preventing the roller submersion in water. In our model (Fig. 1), we preserve only this third layer, formed by the $SCH_2CH_2CH_3$ chains attached to the (empty) coarse grained core that is locally and transiently charged on its surface.

Realistic rollers could be rotated by excitation of their chromophores with a light beam tilted with respect to the water surface. Because of the long wavelengths of light, $\lambda \approx 500$ nm, there is no significant shadowing of the chromophores by the nanorod. However, the chromophores are oriented on average in the radial direction, away from the roller axis. Therefore, their dipolar excitation around the nanorod circumference has a $\cos^2(\theta)$ dependence, where θ is the angle relating the chromophore orientation to the propagation direction of the light beam. Plasmon excitations of the metal nanorod can cause additional asymmetry in the local light field present around its circumference [18–21], which could be further exploited in the nanorod driving.

Coulombic attraction of the transiently and asymmetrically polarized or charged chromophores in these rollers to the highly polar molecules of water should cause unidirectional reorientation (rolling) of the rollers. The charge relaxation time in the chromophores should be matched to the rotation speed of the rollers. A variety of chromophores (xanthene derivatives, tetramethyl rhodamine, fluorescein dyes) is appropriate for such use, since they are

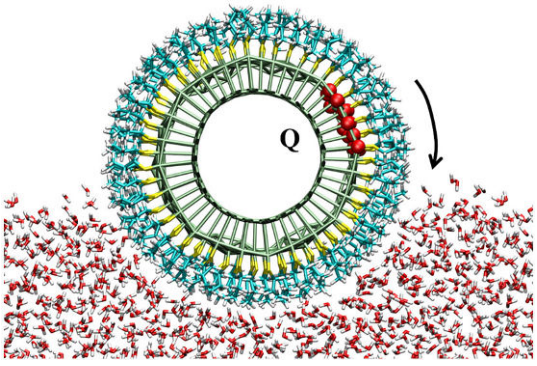


FIG. 1 (color online). Model nanorod rolling on the water surface by Coulombically induced torque (see movie in Ref. [31]).

 © 2009 The American Physical Society

highly polarized upon light excitation and have suitable lifetimes of $\tau_{\text{chrom}} \approx 1$–$4$ ns [22].

We simulate the dynamics of model rollers by classical molecular dynamics with the NAMD package [23] and the CHARMM27 force field [24]. The surfactants on the rollers are described either atomistically (AT) (Fig. 1) or in a coarse grained (CG) form, giving shorter simulations (inset in Fig. 4). In the CG cases, studied more extensively, the core beads are arranged in a stretched hexagonal cell, while the surfactant beads are closely packed in a regular hexagonal cell, forming the outermost layer. This allows one-to-one bonding of surfactant and core beads. The core is formed by two layers of 312 core beads ($m_{\text{bead}} = 50$ Da), arranged as a cylinder with the length of $l_1 = 24$ Å and the external diameter of $d_1 \approx 25$ Å. Its core is kept rigid by the bead parameters ($k_{\text{bond}} = 455$ kcal/mol/Å^2, $k_{\text{angle}} = 35$ kcal/mol/rad^2, dihedrals disabled). We model infinitely long rollers by imposing periodic boundary conditions on the system and connecting cylinders from the neighboring cells by a narrow protrusion ($l_2 = 11.5$ Å, $d_2 = 17$ Å), filling the core of the roller.

The surfactant-covered AT roller and CG roller have the diameters of $D_{\text{AT}} \approx 38$ Å and $D_{\text{CG}} \approx 35$ Å, respectively. In both systems, the van der Waals (vdW) interaction between the surfactant and water atoms is described by the Lennard-Jones potential

$$V_{\text{LJ}}(r_{ij}) = \varepsilon_{ij}\left[\left(\frac{R_{\text{min},ij}}{r_{ij}}\right)^{12} - 2\left(\frac{R_{\text{min},ij}}{r_{ij}}\right)^{6}\right]. \qquad (1)$$

Here, $R_{\text{min},ij}$ is the sum of the radii of particles i and j, and r_{ij} is the distance between the centers of the particles i and j. $\varepsilon_{ij} = \sqrt{\varepsilon_i \varepsilon_j}$ is the depth of the potential well for the interaction of particles i and j, with the ε_i and ε_j contributions, respectively [25]. Water is modeled atomistically and kept flexible. We assume that the dynamics of CG rollers is not dramatically influenced by the coarse grained nature of the surfactants, as long as the atomistic fluid dynamics is preserved. The roller dynamics is described in the NVT ensemble [25].

We simulate driving of the rollers by adding small rechargeable electrodes on their surfaces: a narrow stripe of beads in a layer adjacent to the core and parallel to the water, is sequentially recharged (see Fig. 1). We test two recharging regimes, where one stripe along the roller circumference is always homogeneously charged with one electron. In the "quasistochastic" (STO) regime, recharging of the stripe shifted counterclockwise by $\theta = \pi/6$ from the actually charged stripe is performed once its angle with the water surface drops below $\pi/6$. In the "periodic" (PER) regime, recharging of the next counterclockwise positioned stripe is realized periodically every t_C, giving a charged wave on the surface.

Once a steady-state rotation of the roller is achieved in either recharging regime, its average angular momentum is $L = \text{const}$. The balance can be characterized by the Boltzmann equation in the form $\dot{L}_{\text{drive}} = \dot{L}_{\text{damp}} \approx L/\tau_L$, where $\dot{L}_{\text{drive}}$ and $\dot{L}_{\text{damp}}$ are the driving and damping rates of L, respectively, and τ_L is the angular momentum relaxation time [15]. In Fig. 2, we present the average rotational velocity v_{rot} (bottom) and translational velocity v_{tran} (top), obtained for the CG roller in both regimes as a function of the vdW parameter of the surfactant beads, ε_s. We consider first small ε_s to describe the limit of weak binding. In the PER regime, the (ideal) roller should rotate in phase with the recharging wave, which defines its L, independently on ε_s, and gives $\dot{L}_{\text{drive}} \propto 1/\tau_L$. Therefore, $v_{\text{rot}} \propto L$ should be also independent of ε_s. In this regime, the ideal rotation velocities are $v_{\text{rot}} = 6.6$ and 3.3 rad/ns at the recharging times of $t_C = 80$ and 160 ps,

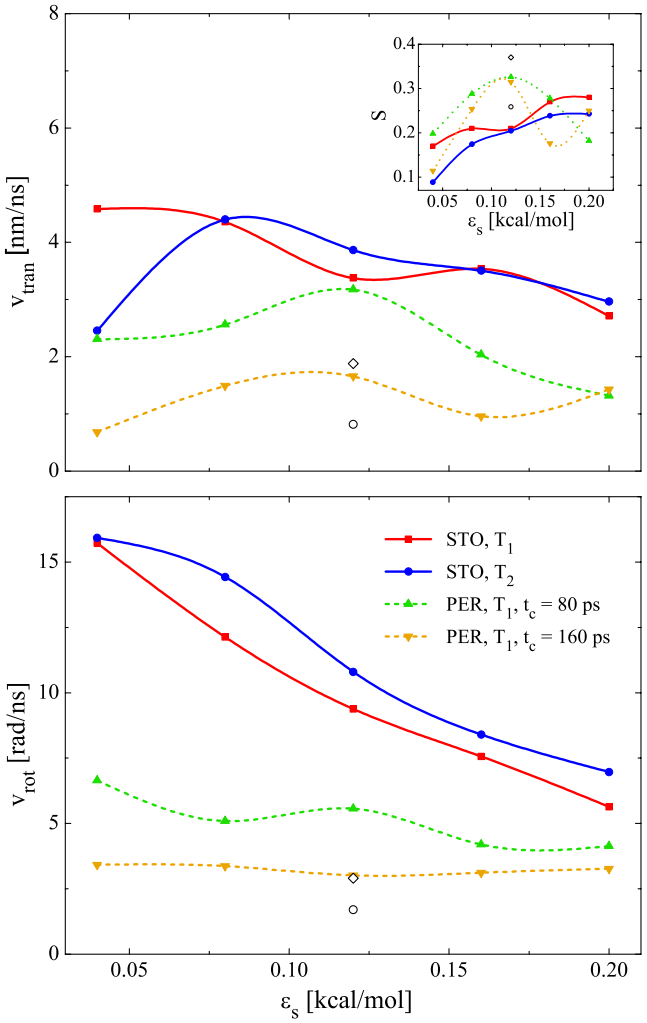


FIG. 2 (color online). (top) The translational v_{tran} and (bottom) rotational v_{rot} velocities of the driven CG roller as a function of the vdW parameter of the surfactant beads, ε_s. The simulation results obtained in the STO and PER recharging regimes are presented at $T_1 = 300$ K and $T_2 = 340$ K. Two points also show the velocities obtained at T_1 for a STO-driven AT roller with alkane surfactants (empty circle) and a CG roller with $\varepsilon_s = 0.57$ kcal/mol (empty diamond), both approximately submerged in the same amount. In the inset (top), the rolling efficiency $S = v_{\text{tran}}/Rv_{\text{rot}}$ is also shown.

respectively. The observed $v_{\rm rot}$ are close to the ideal values, as seen in Fig. 2. At the shorter t_C, the departure from the ideal case is bigger, especially at larger ε_s, where the roller sometimes gets out of phase (freezes).

In the STO regime, we have $\dot{L}_{\rm drive} = |\vec{R} \times \vec{F}|$, where $\vec{F}$ is the average Coulombic force due to the attraction to water of the charged stripe with average positional vector $\vec{R}$. For simplicity, we assume that τ_L decreases with the vdW binding energy of the roller to water [Eq. (1)], $E_{\rm bind} \propto \sqrt{\varepsilon_s}$, so that $\tau_L \propto 1/\sqrt{\varepsilon_s}$. Then, from $L = Iv_{\rm rot} = RF\tau_L$ (I is momentum of inertia), we obtain $v_{\rm rot} = RF\tau_L/I \propto 1/\sqrt{\varepsilon_s}$, in rough agreement with Fig. 2.

In Fig. 2, we also show by two points the results obtained for the AT roller and related CG roller in the STO regime. With $\varepsilon_s = 0.57$ kcal/mol, the CG roller is submerged like the AT roller; typical lipid CG beads have $\varepsilon_s = 0.47$–0.8 kcal/mol [28]. Their $v_{\rm rot}$ velocities are substantially smaller than those obtained at $\varepsilon_s = 0.05$–0.2 kcal/mol, but they roughly fit the dependence of $v_{\rm rot} \propto 1/\sqrt{\varepsilon_s}$. In the PER regime, we would have to substantially increase the period t_C to keep the roller in phase at this ε_s.

To clarify the obtained $v_{\rm tran}$, we use again the Boltzmann equation that in steady-state cases gives $\dot{p}_{\rm drive} = \dot{p}_{\rm damp} \approx p/\tau_p$, where p is the average linear momentum of the roller with the momentum relaxation time τ_p. From the arrangement of the system, we assume that $\dot{p}_{\rm drive} \propto \dot{L}_{\rm damp}$. In general, $\dot{L}_{\rm damp} \propto L/\tau_L$, so we obtain that $p \propto L\tau_p/\tau_L$. It might be again reasonable to assume that $\tau_p \propto 1/\sqrt{\varepsilon_s}$, which in combination with the previous formula simply gives $v_{\rm tran} \propto v_{\rm rot}$. Since $v_{\rm rot}$ is constant in the PER regime, $v_{\rm tran}$ should also remain constant, in partial agreement with Fig. 2. In the STO regime, we obtain $p \propto RF\tau_p$. Thus, $v_{\rm tran} \propto 1/\sqrt{\varepsilon_s}$, which roughly agrees with $v_{\rm tran}$ in Fig. 2.

In order to correlate the $v_{\rm tran}$ and $v_{\rm rot}$ velocities, we define the *rolling efficiency*, $S = v_{\rm tran}/Rv_{\rm rot}$ ($R = D/2$). An ideal (nonslipping) system has $S \to 1$, but the above cases give $S = 0.1$–0.4 (see the inset in Fig. 2). The correlation is worse for small ε_s, due to increased slipping of the roller weakly coupled to the water surface, not included in the above formulas. The effect is more evident at higher temperatures, $T_2 = 340$ K (STO), and slow rotations, $t_C = 160$ ps (PER). As ε_s becomes larger, S saturates and decreases in the PER regime, but it slowly grows in the STO regime, in which the roller can adjust its rotation to its coupling to water. This is also seen in S obtained in the STO regime for the AT and related CG rollers, with even larger ε_s. The overall increase of S with ε_s is caused by the decreased slipping and increased traction of the roller [29].

In Fig. 3, we consider the PER regime and examine dephasing of the CG roller with the recharging frequency. We plot $v_{\rm rot}$ as a function of t_C, and compare the results with the ideal rotation velocity $v_{\rm ideal} = 2\pi/(12t_C)$. At long t_C, the rotation is close to the ideal solution in most systems, since the roller has enough time to adjust itself (adiabatic regime). At shorter t_C, the roller sometimes misses one recharging event and freezes for one charging cycle going around its circumference. This discreteness is also seen from the fact that the nonideal solutions often go in parallel with and at the same distance from the ideal one. Eventually, as $t_C \to 0$, the roller gets completely out of phase, which is accompanied by a drastic drop of $v_{\rm rot}$. The "heavy roller" with core beads of the mass of $m = 400$ Da has almost constant $v_{\rm rot}$, except in the limit of long t_C, showing the absence of locking.

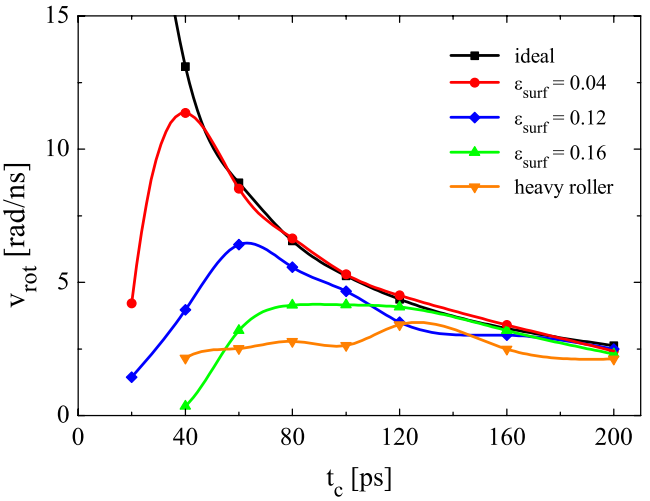


FIG. 3 (color online). The angular velocity $v_{\rm rot}$ of the CG roller as a function of the recharging time t_C.

In Table I, we also present the temperature dependence of $v_{\rm tran}$, $v_{\rm rot}$ and S for rollers driven by a constant torque of $\tau = 8.34 \times 10^{-2}$ nN nm. At low temperature, $T = 280$ K, the AT roller "freezes" to the water surface and S is small. At higher temperature, it is thermally released, which leads to a monotonic increase of $v_{\rm rot}$ and $v_{\rm tran}$, and saturation of $S \approx 0.34$. We also present the results for the CG roller at increasing ε_s and $T = 300$ K. Both velocities dramatically drop with the roller submersion, but the efficiency grows up to $S \approx 0.43$ at $\varepsilon_s \approx 1$ kcal/mol, since the slipping is reduced. At larger ε_s, the roller becomes increasingly buried, it has to push a lot of water to move, and its

TABLE I. (top) The temperature dependence of $v_{\rm tran}$, $v_{\rm rot}$ and $S = v_{\rm tran}/Rv_{\rm rot}$ of the AT roller driven by a constant torque of $\tau = 8.34 \times 10^{-2}$ nN nm. (bottom) The ε_s (in kcal/mol) dependence of the CG roller driven in the same way at $T = 300$ K. For this highly submerged CG roller, the depth of water is increased from $d_w \approx 3.5$ nm to 5.5 nm.

Model/T [K], ε_s	$v_{\rm rot}$ [rad/ns]	$v_{\rm tran}$ [nm/ns]	S
AT/280	4.4	1.6	0.20
AT/300	5.4	3.4	0.33
AT/340	8.1	5.2	0.34
CG/0.1	39.7	15.9	0.23
CG/0.6	9.0	4.9	0.31
CG/1.0	5.1	3.9	0.43
CG/1.2	3.7	1.6	0.25

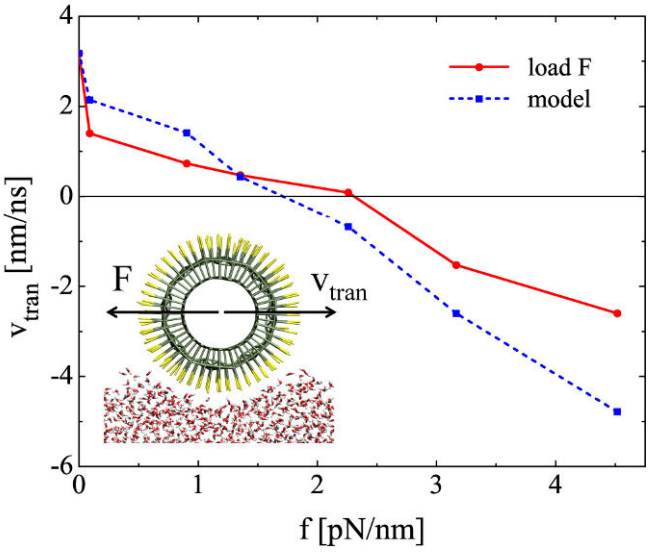


FIG. 4 (color online). The translational velocity v_{tran} of the CG roller with $\varepsilon_s = 0.12$ as a function of the force density f applied to unit length of the roller.

efficiency drops. The efficiency would increase only for less submerged rollers with larger diameters.

We can relate the roller slipping on the liquid surface to the fluid slipping between two moving flat solid walls [30]. In the latter system the slip length b can be linked to the contact angle θ between the liquid and solid by $b \propto 1/(1 + \cos(\theta))^2$, which leads to the divergence of $b \propto \varepsilon_s^{-2}$ at $\varepsilon_s \to 0$ [30]. In this limit, the two types of systems become similar, due to small contact of the roller with water. Here, the simulations give $S \propto \varepsilon_s \propto 1/\sqrt{b}$ (inset in Fig. 2), so the diverging slip length b could be associated with the low rolling efficiency S at $\varepsilon_s \to 0$.

Finally, we test the power of the roller to pull objects attached to it. We apply a loading force F on the roller, which is orthogonal to its axis and parallel to the water surface (inset of Fig. 4). In Fig. 4, we present the obtained dependence of the translational velocities v_{tran} of the CG roller with $\varepsilon_s = 0.12$ on the force density $f = F/l$, where F is the applied force, and $l = 24$ Å is the roller length. The simulations are performed in the PER regime, with $t_C = 80$ ps. We compare v_{tran} obtained with those calculated from $v_{tran}^{model} = v_{tran}^0 + v_{tran}^F$. Here, v_{tran}^0 is the translational velocity of the driven roller with no loading force, and v_{tran}^F is the translational velocity of the nondriven roller with the force F applied to it, which is allowed to translate but not to rotate. The model system resists more the load at small force f, but its velocity drops faster at larger f.

We thank Preston Snee for discussions about experimental realization of the systems. The simulations were performed at the NERSC and NCSA supercomputers.

*pkral@uic.edu

[1] R. Bru, A. Sanchez-Ferrer, and F. Garcia-Carmona, Biochem. J. **310**, 721 (1995).
[2] R. D. Valle and R. A. Milligan, Science **288**, 88 (2000).
[3] A. Gennerich and R. D. Valle, Curr. Opin. Cell Biol. (to be published).
[4] J. S. Berg, B. C. Powell, and R. E. Cheney, Mol. Biol. Cell **12**, 780 (2001).
[5] M. P. Hughes, Nanotechnology **11**, 124 (2000).
[6] M. Durr, J. Kentsch, T. Muller, T. Schnelle, and M. Stelzle, Electrophoresis **24**, 722 (2003).
[7] Y. Lin, H. Skaff, T. Emrick, A. D. Dinsmore, and T. P. Russell, Science **299**, 226 (2003).
[8] R. E. Holmlin, M. Schiavoni, C. Y. Chen, S. P. Smith, M. G. Prentiss, and G. M. Whitesides, Angew. Chem., Int. Ed. Engl. **39**, 3503 (2000).
[9] B. Wang and P. Král, Phys. Rev. Lett. **101**, 046103 (2008).
[10] J. P. Huang, K. W. Yu, G. Q. Gu, and M. Karttunen, Phys. Rev. E **67**, 051405 (2003).
[11] G. J. Simpson, C. F. Wilson, K.-H. Gericke, and R. N. Zare, Chem. Phys. Chem. **3**, 416 (2002).
[12] A. Titov and P. Král, Nano Lett. **8**, 3605 (2008).
[13] B. Wang and P. Král, Phys. Rev. Lett. **98**, 266102 (2007).
[14] E. M. Purcell, Am. J. Phys. **45**, 3 (1977).
[15] B. Wang, L. Vuković, and P. Král, Phys. Rev. Lett. **101**, 186808 (2008).
[16] R. D. Astumian, Science **276**, 917 (1997).
[17] H. Moon, A. R. Wheeler, R. L. Garrell, J. A. Loo, and C.-J. Kim, Lab Chip **6**, 1213 (2006).
[18] H. J. Huang, C. P. Yu, H. C. Chang, K. P. Chiu, H. M. Chen, R. S. Liu, and D. P. Tsai, Opt. Express **15**, 7132 (2007).
[19] C. J. Orendorff, L. Gearheart, N. R. Jana, and C. J. Murphy, Phys. Chem. Chem. Phys. **8**, 165 (2006).
[20] E. K. Payne, K. L. Shuford, S. Park, G. C. Schatz, and C. A. Mirkin, J. Phys. Chem. B **110**, 2150 (2006).
[21] K. L. Shuford, M. A. Ratner, and G. C. Schatz, J. Chem. Phys. **123**, 114713 (2005).
[22] D. Magde, R. Wong, and P. G. Seybold, Photochem. Photobiol. **75**, 327 (2002).
[23] J. C. Phillips *et al.*, J. Comput. Chem. **26**, 1781 (2005).
[24] A. D. MacKerell *et al.*, J. Phys. Chem. B **102**, 3586 (1998).
[25] The cutoff for $V_{LJ}(r_{ij})$ potentials is 14 Å. The force field parameters for the roller are added to the CHARMM27 force field. The depth of the water box, $d_w \approx 3.5$ nm, is maintained by a layer of fixed dummy atoms ($\varepsilon = 0.06$ kcal/mol, with surface density ≈ 24 Å^2 per atom). Electrostatic forces are computed by the particle-mesh Ewald method [26]. Langevin dynamics is used with the damping coefficient of 0.01 ps^{-1} (avoid unphysical momentum dissipation) [27] and the time step is 2 fs.
[26] T. Darden, D. York, and L. Pedersen, J. Chem. Phys. **98**, 10 089 (1993).
[27] J. Servantie and P. Gaspard, Phys. Rev. Lett. **91**, 185503 (2003).
[28] S. J. Marrink, A. H. de Vries, and A. E. Mark, J. Phys. Chem. B **108**, 750 (2004).
[29] R. R. Agayan, R. G. Smith, and R. Kopelman, J. Appl. Phys. **104**, 054915 (2008).
[30] D. M. Huang, C. Sendner, D. Horinek, R. R. Netz, and L. Bocquet, Phys. Rev. Lett. **101**, 226101 (2008).
[31] See EPAPS Document No. E-PRLTAO-103-122952 for a supplementary movie. For more information on EPAPS, see http://www.aip.org/pubservs/epaps.html.